



### Science Arts & Métiers (SAM)

is an open access repository that collects the work of Arts et Métiers Institute of Technology researchers and makes it freely available over the web where possible.

This is an author-deposited version published in: <https://sam.ensam.eu>  
Handle ID: <http://hdl.handle.net/10985/7176>

#### To cite this version :

Eliane GIRAUD, Frederic ROSSI, Guénaël GERMAIN, Jose Carlos MARTINS DO OUTEIRO - Constitutive Modelling of AZ31B-O Magnesium Alloy for Cryogenic Machining - In: 14th CIRP Conference on Modeling of Machining Operations (CIRP CMMO), Italy, 2013-06-14 - Elsevier Procedia CIRP System - 2013

Any correspondence concerning this service should be sent to the repository

Administrator : [scienceouverte@ensam.eu](mailto:scienceouverte@ensam.eu)



## Constitutive Modelling of AZ31B-O Magnesium Alloy for Cryogenic Machining

E. Giraud<sup>a\*</sup>, F. Rossi<sup>b</sup>, G. Germain<sup>a</sup>, J.C. Outeiro<sup>b</sup>

<sup>a</sup> LAMPA, Arts et Metiers ParisTech, Angers, 49000, France

<sup>b</sup> LaBoMaP, Arts et Metiers ParisTech, Cluny, 71250, France

\* Corresponding author. Tel.: +3-324-120-7394 ; fax: +3-324-120-7320 .E-mail address: eliane.giraud@ensam.eu

---

### Abstract

The success of a FE model for metal cutting process is strongly dependent on the accurate characterization of the workpiece material, under similar conditions as those found in metal cutting. In this paper, dynamic shear tests using a Gleeble machine have been performed on 4 mm thickness disks of AZ31B-O magnesium alloy, using a special designed tool. In order to include the effects of the cryogenic cooling in the material behavior, the specimens have been submitted to temperatures ranging from -25°C to 400°C. A Johnson-Cook constitutive model has then been identified in order to describe the flow stress in machining.

© 2013 The Authors. Published by Elsevier B.V.

Selection and/or peer-review under responsibility of The International Scientific Committee of the 14th CIRP Conference on Modeling of Machining Operations" in the person of the Conference Chair Prof. Luca Settineri

*Keywords:* Magnesium alloy; constitutive modelling; cryogenic; machining

---

### 1. Introduction

Cutting process improvement can not be performed without a precise understanding of the chip and machined surface formation. Numerical simulation is a common way to understand and optimize these operations. The success of the model is dependent on the boundary and on the thermomechanical properties of the materials. But the problem is relatively complex since the material behavior is sensitive to the temperature and to the high shear rate observed in chip formation. The knowledge of the mechanical behavior of the alloy under thermomechanical conditions similar to those encountered in cutting process is therefore essential in order to develop a correct numerical simulation.

Mechanical behavior of AZ31B-O alloy under dynamic conditions have already been studied but these works are generally restricted to compressive or tensile loading [1] [2] [3] [4] [5]. They show that two different phenomena can occur during the deformation of the alloy: (i) dislocation glide and twinning and (ii) dynamic recrystallization. Depending on temperature and strain rate, one of these phenomena can be predominant compared to the other leading to some differences in the mechanical response of the material. Therefore, the aim of this work consists in characterizing the shear deformation behavior of 4mm thick AZ31B-O sheet material over a wide range of strain rates from  $10\text{s}^{-1}$  to  $5.10^4\text{s}^{-1}$  and at different temperatures from -25°C to

400°C in order to be representative of thermomechanical conditions encountered during cryogenic machining. Microstructure analysis is also performed to identify the possible deformation mechanisms due to strain rate and temperature. A standard Johnson-Cook model is finally suggested.

### 2. Experimental Setup

A shear test apparatus has been specially designed and developed at the author's laboratory. A schematic view of this apparatus is shown in Fig 1a. It consists of a flat cylindrical punch exhibiting a translatory movement, a blank holder, a die and a specimen. Punch and die diameters are respectively about 9.98mm and 10.02mm. Small disc specimen of 30mm diameter and 4mm thickness has been affixed between the blank holder and the die. Test has then been performed by forcing the flat cylindrical punch through the specimen with an adjustable displacement rate. A shear zone is thus generated into the specimen at the punch/die junction as illustrated in Fig 1b.

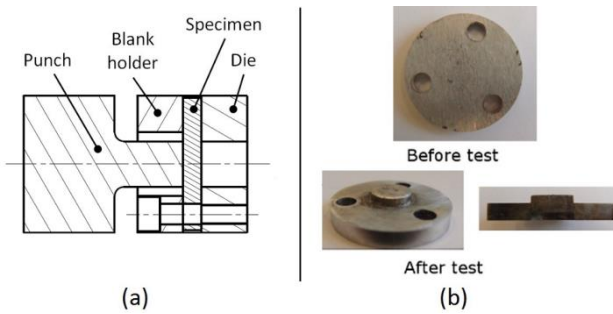


Fig. 1: (a) schematic view of the shear test apparatus; (b) specimen shape before and after deformation

This shear test apparatus has been affixed to a Gleeble 3500 machine in order to pilot punch displacement and specimen temperature. Punch displacement is thus linked to the crosshead displacement of the Gleeble machine. The specimen is heated by Joule effect at 5K/s until the desired temperature. The temperature has been measured by a K-type thermocouple welded in the central part of the specimen and has been monitored in real time to get close to the desired thermal cycle.

Shear tests at various temperatures between  $-25^{\circ}\text{C}$  and  $400^{\circ}\text{C}$  with displacement rates ranging from 0.2 to 1000mm/s have been performed. It can be noticed that one negative temperature (it means  $-25^{\circ}\text{C}$ ) has been studied. For this temperature, the shear test apparatus (specimen included) has been frozen prior its fixing into the Gleeble machine.

Microstructures before and after deformation have been studied for each tested configuration by using optical microscopy in order to underline any microstructural evolutions. After being cut by half (Fig 1b), shear test specimens have been prepared by first a cold mounting. Then, they have been mechanically polished up to 40000 grit SiC paper. Final polishing has been performed on a felt with alcohol lubricant, using 3 microns, 1 microns and finally 0.02 microns silica suspension. Specimens have been then etched with an acetic and picric acid solution.

### 3. Experimental Results And Discussion

#### 3.1. Initial microstructure

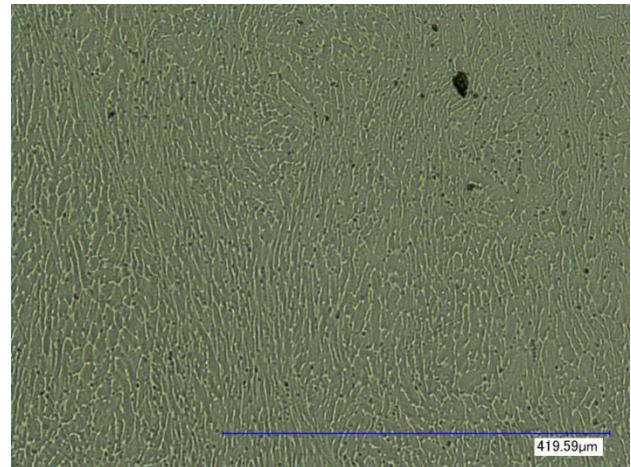


Fig. 2: dendritic structure of the sample (observed without etching)

The specimen alloy is composed of a dendritic structure with  $\alpha$  Mg solid solution formed during the first steps of the cast solidification (chemical composition of the alloy is presented in table 1). Between the dendritic arms, an eutectic compound is formed due to the segregation of Al and Zn (Fig 2). It can be noted that this dendritic microstructure is quite original compared to the equiaxed structure generally studied in the literature [1] [5] [6] [7].

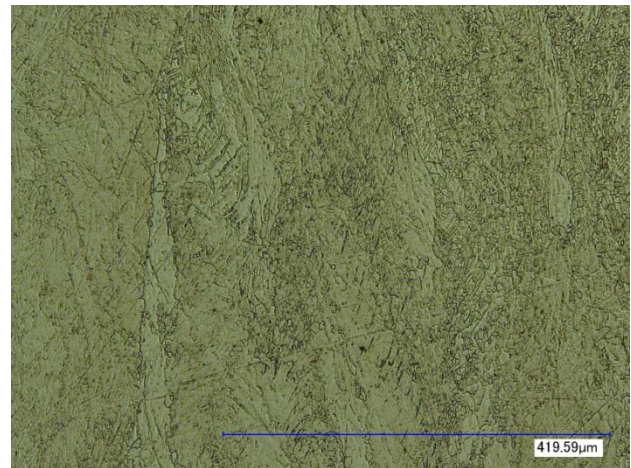


Fig. 3: grain boundaries (observed after etching)

Observations of new grain boundaries surimposed to the solidification dendritic structure are observed on Fig 3 and 4. These partially recrystallized zones are probably due to the rolling process of the magnesium sheet after the casting.

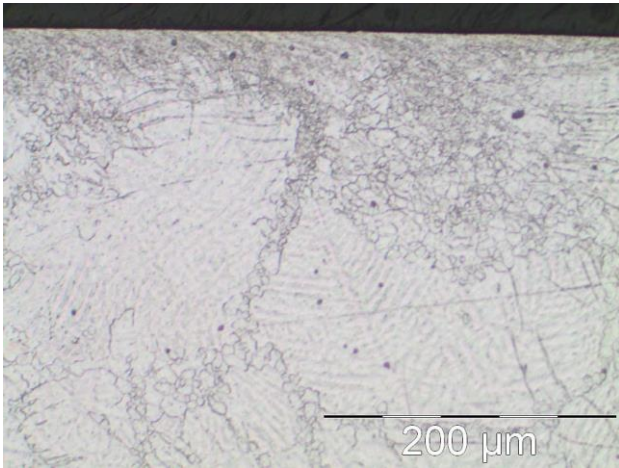


Fig. 4: dendritic and recrystallized grains cohabiting in the sample (observed after etching)

Table 1. Chemical composition of the AZ31B-O alloy

Al (wt%)	Zn (wt%)	Mn (wt%)	Zr (wt%)	Cu (wt%)	Si (wt%)
3.62	0.428	0.365	0.001	0.0021	0.247
Fe (wt%)	Ni (wt%)	Ca (wt%)	Sn (wt%)	Pb (wt%)	Mg (wt%)
0.0034	<0.001	<0.001	<0.005	<0.005	<95.6

### 3.2. Mechanical behavior

Five temperatures have been studied: -25, 25, 200, 300 and 400°C. Four displacement rates have been used: 0.2, 2.2, 60 and 1 000 mm/s. The strain rate reached into the shear zone can be deduced from the applied displacement rate using the following equation:

$$\dot{\gamma} = \frac{\dot{d}}{r_d - r_p} \quad (1)$$

Where:  $\dot{\gamma}$  is the strain rate into the shear zone,  $\dot{d}$  is the displacement rate of the punch,  $r_d$  is the radius of the die and  $r_p$  is the radius of the punch.

The load-displacement data can be converted into stress-strain data using a similar approach that the one developed by Goyal et al. [8]. Stress and strain are thus given by the following expressions:

$$\sigma = \sqrt{3} \cdot \tau = \frac{\sqrt{3} \cdot F}{\pi \cdot (r_d + r_p) \cdot t} \quad (2)$$

$$\varepsilon = \frac{\gamma}{\sqrt{3}} = \frac{d}{\sqrt{3} \cdot t} \quad (3)$$

Where:  $\sigma$  is the equivalent stress,  $\tau$  is the shear stress,  $F$  the force,  $t$  the specimen thickness,  $\varepsilon$  the equivalent strain,  $\gamma$  the shear strain and  $d$  the displacement of the punch. Stress-strain curves have been corrected to take

into account the stiffness of the test apparatus and of the Gleeble crosshead. For each temperature, the stiffness of the device has been determined so that the slope of the elastic part of the experimental curve corresponds to the elastic modulus of the material found by Hama et al. [9].

### Influence of temperature

From stress-strain curves shown in Fig 5, two points can be underlined: (i) the flow stress decreases with the increasing test temperature and (ii) the alloy exhibits different behaviors when the temperature is inferior or superior to 200°C. Indeed, during the deformation, an initial strain hardening stage occurs followed by a strain softening stage more or less important.

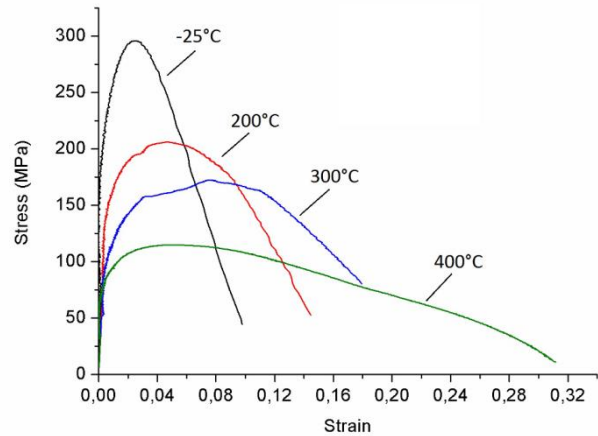


Fig. 5: stress-strain curves obtained after shear tests performed within a vast range of temperatures with a strain rate of 4.103s<sup>-1</sup>

For temperatures higher than 200°C, the material exhibits a softening behavior that is not very pronounced at -25°C. Indeed, for this temperature, the curve exhibits a different shape: stress increases strongly until a peak value from which damage occurs almost immediately leading to a fast decrease in stress. This difference in the mechanical response can be explained by the activation of different phenomena during the deformation. For temperatures inferior to 200°C, deformation by dislocation glide and twinning occur whereas, for temperatures superior to 200°C, dynamic recrystallization is predominant. This change in the mechanical response as a function of temperature has been already underlined by Ulacia et al. [1]. They have found a transition temperature about 150°C but under quasi-static conditions (i.e. strain rates inferior to 0.1s<sup>-1</sup>). Thus, this transition occurs even at high strain rates but the gain in strain to failure brought by the softening phenomenon is less pronounced. The increase in the strain to failure, at high strain rates, when increasing temperature, is indeed three times less important than the one found by Ulacia et al. [1] at low strain rates.

*Influence of strain rate*

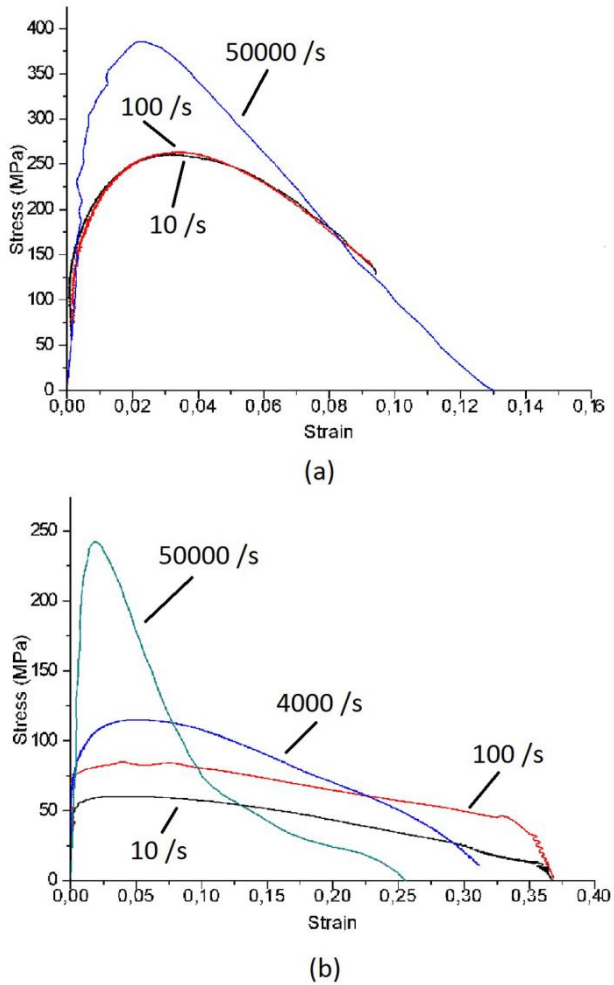


Fig. 6: stress-strain curves obtained after shear tests performed within a vast range of strain rates at a temperature of 25°C (a) and 400°C (b)

From stress-strain curves shown in Fig 6, It can be seen that the mechanical response of the alloy is different when increasing strain rate depending on the test temperature (inferior or superior to 200°C) i.e. depending on the phenomena which are activated during the deformation. For temperatures inferior to 200°C, the flow stress sensitivity to strain rate is quite limited: an increase in stress is only obtained for the highest rate (i.e.  $5 \cdot 10^4 \text{s}^{-1}$ ). Moreover, the increase in strain rate does not modify the deformation mechanisms which are always linked to dislocation glide and twinning. For temperatures superior to 200°C, an increase in yield and flow stresses are obtained when increasing strain rate. Stress sensitivity to strain rate is thus more significant. It can also be underlined that the alloy loses its softening behavior when strain rate exceeds  $4 \cdot 10^3 \text{s}^{-1}$ . This is probably due to the fact that the time period over which the deformation occurred at the highest strain rate is significantly shorter than that required for dynamic

recrystallization to occur. However, it is quite surprising to have dynamic recrystallization within the strain rate range used in this study. The contribution of rotational recrystallization mechanism as suggested by Ulacia et al. [10] can maybe explain this point.

*3.3. Microstructural evolutions*

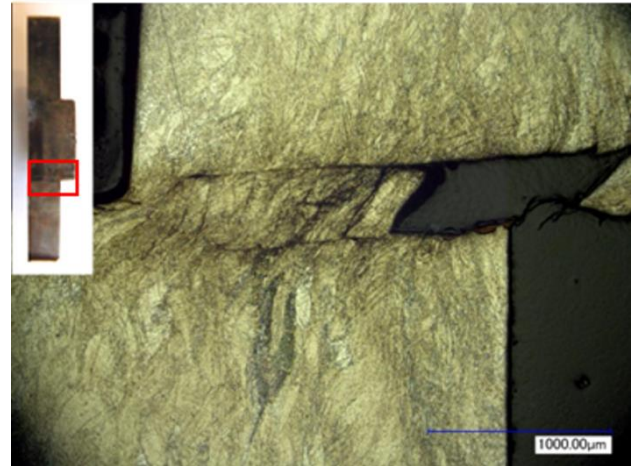


Fig. 7: microstructural observation after a shear test performed with a strain rate of 10s-1 at room temperature

Some microstructural observations of the shear zone have been carried out in order to underline the possible deformation mechanisms. From Fig 7 and 8, it can be seen that a localization of the plastic deformation occurs with the decreasing test temperature. For temperatures inferior to 300°C and low shear rates, the thickness of the plastified zone is minimal and around 0.1 mm. Two parallel fractures are also often observed (Fig 7). For high temperature and high shear rate, the zone of plastic deformation is four times larger, as shown in Fig 8.

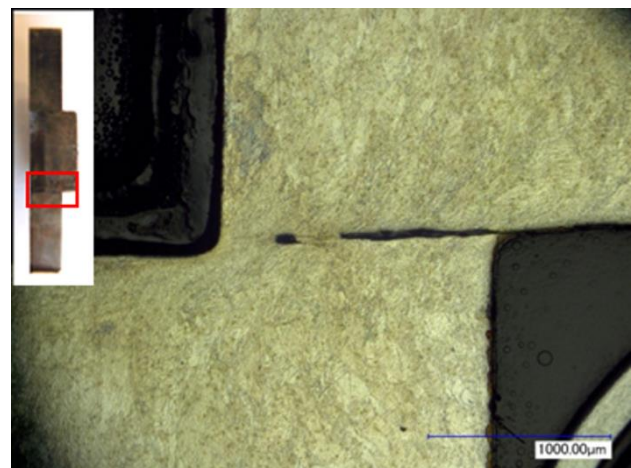


Fig. 8: microstructural observation after a shear test performed with a strain rate of 5.104s-1 at a temperature of 400°C

However, microstructural observations by using optical microscopy do not allow detecting crystal twinning due to the small size of the shear zone. But, some microstructural refinement has been observed on the microstructures obtained after shear tests at high temperatures.

### 3.4. Modeling of the shear behavior

To model the constitutive response of the material, the flow stress has been determined as a function of the plastic strain, the strain rate and the temperature using the empirical law of Johnson-Cook [11]:

$$\sigma = [A + B \cdot \epsilon^n] \cdot \left[ 1 + C \cdot \ln\left(\frac{\dot{\epsilon}}{\dot{\epsilon}_0}\right) \right] \cdot \left[ 1 - \left(\frac{T - T_0}{T_m - T_0}\right)^m \right] \quad (4)$$

Where: A, B, C, n and m are the model parameters.  $T_m$  is the melting temperature of the alloy (equal to 630°C and taken from Avedesian et al. [12]).  $T_0$  and  $\dot{\epsilon}_0$  are respectively a reference temperature (-25°C) and a reference strain rate ( $10s^{-1}$ ). A, B and n have been determined by using the curve obtained at the reference temperature and strain rate. A corresponds to the elastic limit of the alloy while B and n correspond respectively to the origin and the slope of the curve  $\ln(\sigma - A)$  vs.  $\ln(\epsilon)$ . C and m are then identified for each condition of temperature and strain rate by using a Newton-Raphson solver. C and m correspond thus to an average value. Table 2 summarizes the values of the different parameters of the Johnson-Cook law.

Table 2. Parameters of the Johnson-Cook law

A (MPa)	B (MPa)	n	C	m
100	380	0.28	0.04	1.04

By applying the Johnson-Cook law, it can be noticed that the model does not correctly fit experimental data for each studied configuration. As shown in Fig 9, the model works relatively well for low strain rates (i.e. for  $\dot{\gamma} < 4 \cdot 10^3 s^{-1}$ ) whatever the temperature considered. But for high strain rates, differences between modeled and experimental data are more and more pronounced when increasing temperature. These differences can, for instance, exceed 30% for the curve obtained at 25°C with a strain rate of  $5 \cdot 10^4 s^{-1}$ . It can be explained by the fact that constant parameters are used, which is not appropriate since the alloy exhibits different behaviors depending on temperature and strain rate as explained in previous paragraphs. Stress sensitivity to strain rate is important at high temperatures but small at low temperatures and softening mechanism is predominant at high temperatures. Consequently, to better fit experimental data, it would in fact be necessary to take

into account the behavior evolution when changing temperature and strain rate. Therefore, parameters set specific to each configuration has to be employed. Moreover, damage is not taken into account leading to a continuous increase in stress during plastic deformation. It would in fact be necessary to identify a damage criterion to describe the stress decrease. This study will be done in future works by performing mechanical tests on samples exhibiting various triaxiality ratios.

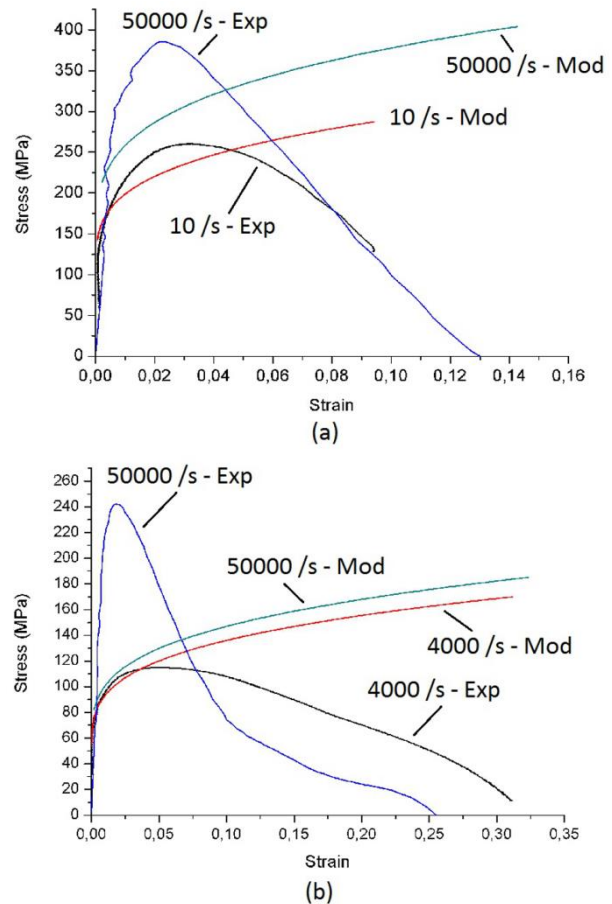


Fig. 9: (a) comparison between experimental and modeled curves obtained at 25°C and (b). 400°C

## 4. Conclusions

The shear behavior of an AZ31B-O magnesium alloy has been investigated for temperatures and strain rates representative of thermomechanical conditions encountered during cryogenic machining. An original shear test apparatus has been developed and inserted into a Gleeble machine. Temperatures ranging from -25 to 400°C have been studied as well as strain rates ranging from 10 to  $5 \cdot 10^4 s^{-1}$ . Results show that the mechanical behavior for  $T < 200^\circ C$  differs from the one obtained for  $T > 200^\circ C$ . For  $T < 200^\circ C$ , stress does not seem

sensitive to strain rate and the alloys deforms by dislocations glide and twinning. For  $T > 200^{\circ}\text{C}$ , stress is sensitive to strain rate and the alloys exhibits a softening behavior due to dynamic recrystallization. However, this point is not verified for the highest strain rate (i.e.  $5 \cdot 10^4 \text{s}^{-1}$ ) for which the alloy does not exhibit a softening behavior. Microstructural observations of the shear zone have shown the localization of the deformation for low temperatures. But they have not allowed detecting the different deformation mechanisms. The use of a Johnson-Cook law to describe the behavior of the alloy within the plastic domain is not adapted since different deformation modes occur and are not taken into account when using constant parameters. Therefore, it will be interesting, in future works, to study another behavior laws as well as appropriate damage criteria to describe the decrease in stress.

## References

- [1] I. Ulacia, C.P. Salisbury, I. Hurtado, M.J. Worswick, 2011, *Journal of materials processing technology*, 211:830-839
- [2] K. Ishikawa, H. Watanabe, T. Mukai, 2005, *Journal of materials science*, 40/7:1577-1582
- [3] T. Mukai, M. Yamanoi, K. Higashi, 2000, *Materials science forum*, 350:97-102
- [4] T. Yokohama, 2003, *Strain*, 39/4:167-175
- [5] E. El-Magd, M. Abouridouane, 2006, *International journal of impact engineering*, 32:741-758
- [6] Z. Pu, J.C. Outeiro, A.C. Batista, O.W. Dillon, D.A. Puleo, I.S. Jawahir, 2011, *Procedia Engineering*, 19:282-287
- [7] Z. Pu, J.C. Outeiro, A.C. Batista, O.W. Dillon, D.A. Puleo, I.S. Jawahir, 2012, *International journal of machine tools and manufacture*, 56:17-27
- [8] S. Goyal, V. Karthik, K.V. Kasiviswanathan, M. Valsan, K. Bhanu Sankara Rao, B. Raj, 2010, *Materials and Design*, 31:2546-2552.
- [9] T. Hama, Y. Kariyazaki, K. Ochi, H. Fujimoto, H. Takuda, 2010, *Materials Transactions*, 51:685-693.
- [10] I. Ulacia, N.V. Dudamell, F. Galvez, S. Yi, M.T. Perez-Prado, I. Hurtado, 2010, *Acta materialia*, 58:2988-2998
- [11] G. Johnson, W. Cook, 1983, *Proceedings 7<sup>th</sup> international symposium on ballistics*, 541-547
- [12] M. Avedesian, H. Baker, 1999, *Magnesium and Magnesium alloys*, ASM specialty handbook, ASM Int., Materials Park, OH.